Petroleum Science 23 (2026) 4914–4926

Contents lists available at ScienceDirect

Petroleum Science

journal homepage: www.keaipublishing.com/en/journals/petroleum-science

Original Paper

Ensemble-based interpretation of partitioning inter-well tracer tests for residual saturation and permeability estimation

Zi-Hao Zhao, Yu-Hao Ou, Cun-Qi Jia, Ruo-Yu Li, Kishore Mohanty *

Hildebrand Department of Petroleum & Geosystems Engineering, The University of Texas at Austin, 200 E. Dean Keeton St, Austin, TX 78712, USA

A R T I C L E I N F O

Article history:
Received 6 August 2025
Received in revised form
17 October 2025
Accepted 10 March 2026
Available online 14 March 2026

Edited by Meng-Jiao Zhou

Keywords:
Inter-well tracers
Partitioning tracers
Data assimilation
Phase saturation
Reservoir characterization

A B S T R A C T

Partitioning inter-well tracer test (PITT) is a direct method for quantifying remaining oil saturation (S_{or}), but conventional interpretation workflows can lead to significant overestimation if neglecting reservoir heterogeneity and mobile oil. This research introduces an advanced numerical workflow that overcomes these limitations by integrating the ensemble smoother with multiple data assimilation (ESMDA) with the UTCHEM reservoir simulator. UTCHEM is used to simulate production rate and tracer profile of each geological realization and ESMDA iteratively refines spatial distributions of both permeability (k) and S_{or} by jointly assimilating production and tracer data simultaneously. The workflow was successfully validated on synthetic reservoir models featuring high-permeability channels and spatially variable S_{or}. To demonstrate its superiority, the results were compared against both a traditional analytical solution and an assimilation case that excluded tracer data. Furthermore, a permeability-weighted S_{or} is proposed to better identify and prioritize oil recovery targets within the reservoir. The results demonstrate that coupling production and tracer data significantly cterization, reducing the estimation error by 86% compared to traditional analytical solutions. Our method yielded 3% error in S_{or} estimation compared to 22%–27% error by the traditional analytical methods. It accurately reconstructs the high-resolution spatial distribution of both k and S_{or}, provides an ensemble of solutions for uncertainty quantification, and is robust against data noise. This ensemble-based workflow offers a powerful technique for improving inter-well characterization, essential for both enhanced oil recovery and the assessment of non-aqueous phase liquid (NAPL) contamination.

1. Introduction

Partitioning inter-well tracer test (PITT) is a hydrological tool for aquifer and reservoir characterization. Initially developed for enhanced oil recovery (EOR) operations, PITTs were designed to measure the remaining oil saturation (S_{or}), which helps to evaluate the feasibility prior to the implementation (Huseby et al., 2015). PITTs also provide critical insights into swept volumes and dominant flow paths (Pu et al., 2016), which are all essential parameters for developing effective reservoir management. Subsequently, PITTs expanded to wider applications such as subsurface nonaqueous phase liquids detection (Hartog et al., 2010), fracture diagnosis (Zhang et al., 2023), and geothermal (Hirtz et al., 2001).

The schematic of PITT is shown in Fig. 1. PITT involves simultaneous injection of both partitioning and non-partitioning tracers in injection wells, transport through a subsurface formation, and production of these tracers in the production wells (Tang and Harker, 1991). During the flow, non-partitioning tracers remain within the mobile water phase, whereas partitioning tracers exhibit an affinity for the nonaqueous phase, causing them to distribute between the mobile water phase and the immobile residual oil phase. The differential partitioning leads to the chromatographic separation and retardation of partitioning tracers during production stage (Suva et al., 2003).

PITTs offer distinct advantages compared to alternative characterization methods, such as single-well tests or core analyses. Most notably, PITTs provide measurements integrated over a significantly larger reservoir volume (>100 ft), yielding more representative assessments of inter-well subsurface conditions

* Corresponding author.
E-mail address: mohanty@mail.utexas.edu (K. Mohanty).

Peer review under the responsibility of China University of Petroleum (Beijing).

https://doi.org/10.1016/j.petsci.2026.03.019
1995-8226/

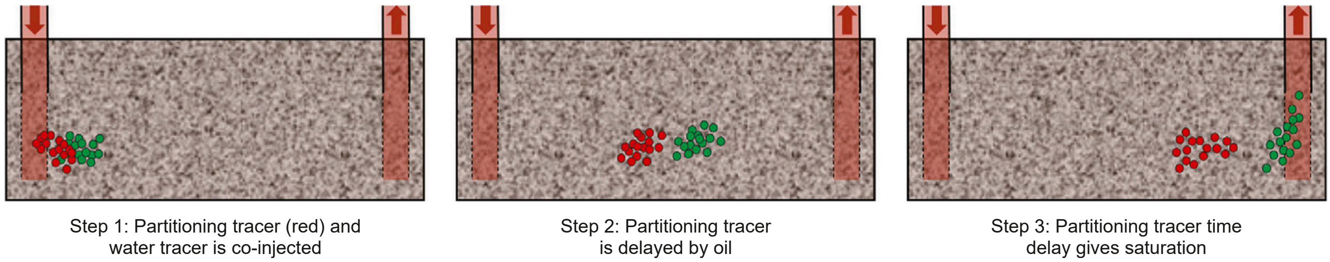

Fig. 1. Chromatographic separation of partitioning tracer (red) and the non-partitioning tracer (green) because of the immobile oil phase during partitioning inter-well tracer test (Sanni et al., 2018).

(Tayyib et al., 2019). This volumetric averaging intrinsically accounts for heterogeneity that might not be fully captured by point-scale measurements (Keller et al., 2023). Additionally, PITTs are non-destructive and minimally invasive that are compatible with all types of EOR (Cubillos et al., 2015). The tests can be conducted under prevailing reservoir flow conditions, providing insights into actual fluid transport behavior and formation connectivity (Sanni et al., 2015).

Various methods exist for interpreting PITT data, ranging from qualitative analysis (Aparecida de Melo et al., 2001), analytical solutions (Brigham and Smith, 1965; Tang, 2005) to numerical simulations (Allison et al., 1991; Illiassov and Datta-Gupta, 2002). One of the most commonly used analytical method is based on the first temporal moments of the tracer breakthrough curves (Jin et al., 1995). Tang (1995, 2005) also proposed a chromatographic transform to interpret the result and incorporate the partitioning tracer model in the Brigham's model (Tang, 2005). Velasco-Lozano (Velasco-Lozano and Balhoff, 2023) proposed an analytical solution for two phase flow tracer transport. Qualitative and analytical solutions are based on simplistic assumptions and are easy to apply. However, its accuracy requires ideal conditions.

The numerical method gets oil distribution between wells derived by matching the tracer production profiles using a 3D finite difference simulator such as UTCHEM or by a streamline model. Accurately accounting for the influence of reservoir heterogeneities is crucial for a good match, but is often challenging and neglected (Agca et al., 1990; Allison et al., 1991; Saad et al., 1989). High-permeability channels or natural fracture networks can lead to early tracer breakthrough, while low-permeability zones or stagnant areas may cause pronounced tracer tailing and delayed production (Dwarakanath et al., 1999). Numerical method suffers from the non-uniqueness solutions due to the complex flow path in the heterogeneity formation.

Automated history matching techniques can efficiently samples the solution space and provide high resolution result are widely applied in petroleum industry such as Genetic Algorithms, Differential Evolution and Particle Swarm Optimization (Liu et al., 2023; Oliver and Chen, 2011; Zhao et al., 2021, 2025). More recently, ensemble-based data assimilation methods, such as EnKF have gained significant prominence (Oliver and Chen, 2011). Guo et al. (2021) applied the EnKF to assimilate the tracer profile for S_{or} estimation and provide a high resolution S_{or} distribution. The ensemble smoother with multiple data assimilations (ESMDA) is a notable advanced ensemble-based technique. ESMDA is an iterative ensemble smoother that assimilates the entire historical dataset multiple times. Unlike sequential data assimilation methods such as the Ensemble Kalman Filter (Gu and Oliver, 2005), which process data sequentially in time, ES-MDA assimilates all historical data simultaneously within each iteration and repeats this assimilation process over several iterations with an error covariance matrix. This approach has demonstrated advantages in achieving a better history match and providing a more reliable quantification of uncertainty compared to some earlier ensemble methods (Zhang et al., 2022). ESMDA's capability to handle non-linear relationships between model parameters and observed data, alongside its capacity to maintain geological consistency within the ensemble members, has established it as a valuable tool in assisted history matching workflows (Evensen et al., 2019).

The applicability of earlier interpretation workflows is compromised by their reliance on a simplified, homogeneous reservoir model with a single permeability and S_{or} value. Critically, these methods also mandate that the reservoir be fully flooded to its residual oil saturation, a condition that is often economically detrimental and delays practical application. The aim of this research is to evaluate the formation heterogeneity and S_{or} by PITT with an efficient interpretation workflow. This work introduces a novel numerical interpretation workflow by integrating the ESMDA algorithm with the UTCHEM reservoir simulator, as shown in Fig. 2. This integration facilitates the iterative updating of permeability and S_{or} by calibrating simulation result with actual field measurements. The resulting posterior ensemble of permeability and S_{or} serves as the interpreted reservoir properties. A key novelty of this workflow lies in its ability to concurrently calibrate both reservoir heterogeneity and oil saturation through the assimilation of diverse data sources, including tracer and production data. Importantly, this workflow remains accurate even when the reservoir has mobile oil ($S_{or} > S_{orw}$), the residual oil

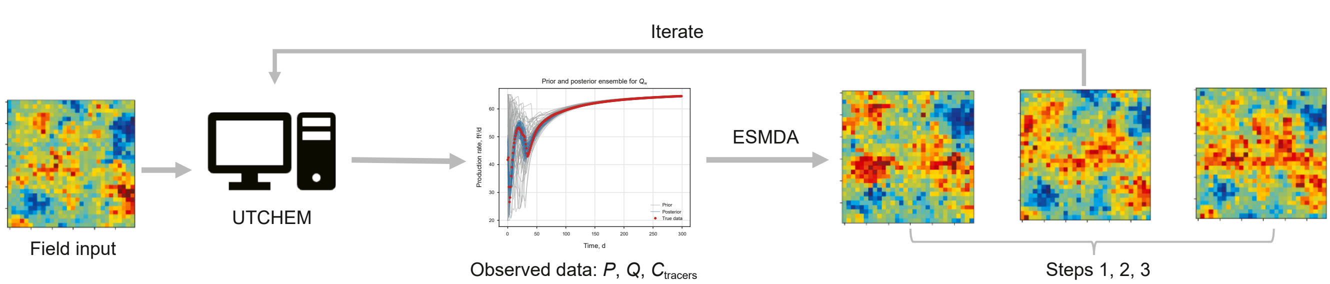

Fig. 2. Interpretation workflow for PITT.

saturation to water flood). The performance of this new interpretation workflow is first evaluated through a synthetic case. Subsequently, its performance is compared against traditional history matching approaches with only production data, highlighting the significance of partitioning tracers. The workflow is then compared with traditional analytical solutions. The validation process also involves assessing the workflow's sensitivity to variations in the data error covariance function.

2. Methodology

2.1. UTCHEM simulator

UTCHEM is a reservoir simulator developed at The University of Texas at Austin to simulate injection of chemicals into reservoirs. It simulates phase behavior of oil, brine, and chemical mixtures, along with convection, diffusion, dispersion, adsorption and reactions. It is explicitly designed and utilized for simulating tracer tests, especially PITT, for reservoir characterization. The core capability lies in modeling complex multiphase phase behavior, flow, and multicomponent reactive transport. The development of the flow equations is based upon several key assumptions.

- Local thermodynamic equilibrium is maintained for all components except for tracers.
- Both the porous rock formation and the reservoir fluids are considered to be slightly compressible.
- Fluid flow is governed by Darcy's law.
- Fluid mixing is assumed to be ideal within a grid block.
- Fluid mixing within a phase between adjacent grid blocks is represented by Fickian diffusion and dispersion.

Some of the key steps of the simulator are described next.

2.1.1. Mass conservation equations

The principle of mass conservation for each component κ is expressed in terms of the overall volume of component κ per unit pore volume, denoted as $\mathscr{V}_\kappa$. The continuity equation for component κ is given by:

$$\frac{\partial(\phi\mathscr{V}_\kappa)}{\partial t}+\nabla\cdot\boldsymbol{F}_\kappa=q_\kappa \tag{1}$$

where $\boldsymbol{F}_\kappa$ is the total flux (convective + dispersive) of component κ, and q_κ represents source or sink terms. The overall volume of component κ per unit pore volume is defined as the sum over all phases j:

$$\mathscr{V}_\kappa=\sum_{j=1}^{n_\mathrm{p}}\frac{\rho_{\kappa j}V_j}{\rho_k^0} \tag{2}$$

In this formulation, the components considered include water, oil, surfactant, and other chemicals. Here, n_p is the number of mobile phases, $\rho_{\kappa j}$ is the mass concentration of component κ in phase j, V_j is the volume of phase j, and ρ_k^0 is the density of pure component κ at standard conditions. $\boldsymbol{u}_l$ is the Darcy velocity of phase l, which is proportional to the pressure gradient:

$$\boldsymbol{u}_l=-\frac{k_{rl}}{\mu_l}\boldsymbol{K}\cdot\nabla P_l \tag{3}$$

where k_{rl} is the relative permeability of phase l. μ_l is the viscosity of phase l. $\boldsymbol{K}$ is the permeability tensor of the medium. P_l is the pressure of phase l. The dispersive flux $\boldsymbol{F}_{\kappa,\mathrm{disp}}$, which contributes to the total flux $\boldsymbol{F}_\kappa$, is assumed to follow a Fickian form:

$$\boldsymbol{F}_{\kappa,\mathrm{disp}}=-\phi\boldsymbol{K}\cdot\nabla\mathscr{V}_\kappa \tag{4}$$

where ϕ is porosity and $\boldsymbol{K}$ is the dispersion coefficient tensor.

2.1.2. Pressure equation

Derivation of the pressure equation involves aggregating the mass balance equations for all components. This aggregate equation is then formulated in terms of phase pressures by substituting the phase flux terms using Darcy's law and incorporating capillary pressure relationships. Taking the water phase pressure as the reference phase pressure, the pressure equation is given by:

$$\frac{\partial\left(\phi\sum_l S_l\rho_l\right)}{\partial t}=-\nabla\cdot\left(\sum_l\rho_l\boldsymbol{u}_l\right)+\sum_k Q_k \tag{5}$$

where ϕ is the porosity. S_l is the saturation of phase l. ρ_l is the density of phase l. t is time, $\boldsymbol{u}_l$ is the Darcy velocity of phase l. Q_k represents the source or sink terms for component k.

2.1.3. Tracer modeling

The simulator incorporates specific modules and options to handle "tracer properties". These include the key mechanisms of partitioning between phases, adsorption onto the rock matrix, radioactive decay for isotopic tracers, chemical reactions such as ester hydrolysis, and capacitance effects modeling diffusion into and out of immobile pore spaces (dead-end pores). For water/oil partitioning tracers, the partitioning coefficient, K_T, is a key parameter defined as the ratio of tracer concentrations:

$$K_\mathrm{T}=\frac{C_\mathrm{o}}{C_\mathrm{w}} \tag{6}$$

where C_o and C_w are the tracer concentrations in the water and oil phases.

2.2. Ensemble smoother with multiple data assimilation

We begin by defining the forward problem, where a numerical model takes a vector of input parameters, $\boldsymbol{m}$, to produce a set of simulated data. The true underlying parameters are unknown. Our goal is to infer these parameters by conditioning the model on a set of noisy observational data, $\boldsymbol{d}$, as shown in Eq. (1):

$$\boldsymbol{d}=g(\boldsymbol{m}^*)+\boldsymbol{\epsilon} \tag{7}$$

Here, $\boldsymbol{\epsilon}$ represents the observation error, which is assumed to follow a zero-mean Gaussian distribution. Following Bayesian theory, we can update our initial understanding of the parameters (the prior distribution, $p(\boldsymbol{m})$) by incorporating the information from the observations. This updated knowledge is captured by the posterior distribution, $p(\boldsymbol{m}|\boldsymbol{d})$, calculated as:

$$p(\boldsymbol{m}|\boldsymbol{d})=\frac{p(\boldsymbol{d}|\boldsymbol{m})p\ (\boldsymbol{m})}{p(\boldsymbol{d})}. \tag{8}$$

In this equation, $p(\boldsymbol{d}|\boldsymbol{m})$ is the likelihood function, which quantifies how probable the observed data $\boldsymbol{d}$ are for a given parameter set $\boldsymbol{m}$. The term in the denominator, $p(\boldsymbol{d})$, is the evidence, which acts as a normalization constant.

For complex and high-dimensional models, the posterior distribution $p(\boldsymbol{m}|\boldsymbol{d})$ is often analytically intractable. We therefore turn to Monte Carlo methods to approximate it. This is done by first generating an ensemble of N_a random parameter samples, $M_0=\{m_i\}_{i=1}^{N_\mathrm{a}}$, drawn from the prior distribution. The numerical model g

is then run for each sample to compute the corresponding model outputs, creating an ensemble of simulated data, $D_0 = \{g(m_i)\}_{i=1}^{N_e}$.

The ESMDA is an iterative method for updating the parameter ensemble. In its simplest, single-iteration form (equivalent to the standard Ensemble Smoother), each parameter sample m_i in the initial ensemble is updated using the Kalman formula:

$$\boldsymbol{m}_i^u = \boldsymbol{m}_i + \boldsymbol{C}_{m_0,D_0}\left(\boldsymbol{C}_{D_0,D_0} + \boldsymbol{C}_D\right)^{-1}(\boldsymbol{d}_i - g(\boldsymbol{m}_i)). \tag{9}$$

where $\boldsymbol{m}_i^u$ is the updated parameter sample. $\boldsymbol{C}_{M_0,D_0}$ is the cross-covariance matrix between the prior parameter ensemble and the simulated data ensemble. $\boldsymbol{C}_{D_0,D_0}$ is the auto-covariance matrix of the simulated data ensemble. $\boldsymbol{d}_i = \boldsymbol{d} + \epsilon_i$ is the observed data perturbed with a random realization of the observation error, ϵ_i.

The key innovation of ESMDA is to apply this update iteratively to better handle highly nonlinear problems. Instead of a single update, the assimilation is performed over N_a steps. At each iteration t, the observation error covariance matrix $\boldsymbol{C}_D$ is inflated by a coefficient α_t :

$$\boldsymbol{m}_{i,t} = \boldsymbol{m}_{i,t-1} + \boldsymbol{C}_{M_{t-1},D_{t-1}}\left(\boldsymbol{C}_{D_{t-1},D_{t-1}} + \alpha_t\boldsymbol{C}_D\right)^{-1}(\boldsymbol{d}_i - g(\boldsymbol{m}_{i,t-1})) \tag{10}$$

The inflation coefficients α_t are chosen such that they satisfy the condition $\sum_{t=1}^{N_a} \frac{1}{\alpha_t} = 1$. This ensures that the total update applied over all iterations is consistent with the single update in Eq. (10). After iterations, the final ensemble, is taken as the approximation of the posterior parameter distribution $p(\boldsymbol{m}|\boldsymbol{d})$.

The workflow for applying ESMDA involves the following steps.

1. **Initialization**: Generate an ensemble of reservoir models (k, S_{or}). Each model in the ensemble represents a possible realization of the reservoir's properties.
2. **Run the ensemble forward**: Run reservoir simulator, UTCHEM for all ensemble members and obtain injector pressure (P_{inj}), water production rate (Q_w) and tracer concentrations ($C_{tracer1}$; $C_{tracer2}$).
3. **Calculate misfit and covariances**: Compare the simulated production data from each ensemble member with the actual historical production data. Estimate the ensemble sample covariance between the model parameters and the simulated data and the covariance of the simulated data itself (data covariance).
4. **Update the ensembles using Eq. (7)**: In each assimilation step m, the historical data is perturbed to calculate the update that is applied to each ensemble member. This perturbation, consistent with the assumed covariance of the measurement errors, allows the ensemble members to explore the parameter space more effectively over the steps.
5. **Repeat forward runs and assimilation**: After updating the model parameters in step 4, run the reservoir simulator forward again for each updated ensemble member. Repeat steps 3 and 4 for the specified number of assimilation steps. With each assimilation step, the ensemble of models should move closer to matching the historical production data.

3. Assimilation results

3.1. Model setup

A two-dimensional synthetic model was created on a 30-by-30 grid, representing a 300 by 300-foot formation. Within this domain, an injector well operating at a constant rate was positioned in the bottom-left corner, while a producer well with constant pressure was placed in the top-right corner as shown in Fig. 3. The simulation's conditions involved the injector operating at a steady rate of 375 ft^3/d and the producer being maintained at 15 psi, all within a formation that had a constant initial pressure of 300 psi. Under such setup, the total production rate at the producer is constantly 375 ft^3/d as well. The model was simulated over a total period of 300 days, with observation data being collected every 24 h.

For simplicity in this specific case, porosity was maintained constant at 0.3, although the proposed workflow is capable of handling variable porosity fields. The k and S_{or} fields for the synthetic model were generated using Gaussian Random Fields with Cholesky Decomposition, followed by the addition of random noise. Permeability values ranged from 0.1 to 1 mD, and S_{or} values were between 0.25 and 0.55. A high-permeability channel was intentionally incorporated between the injector and producer wells to represent a specific geological feature targeted for

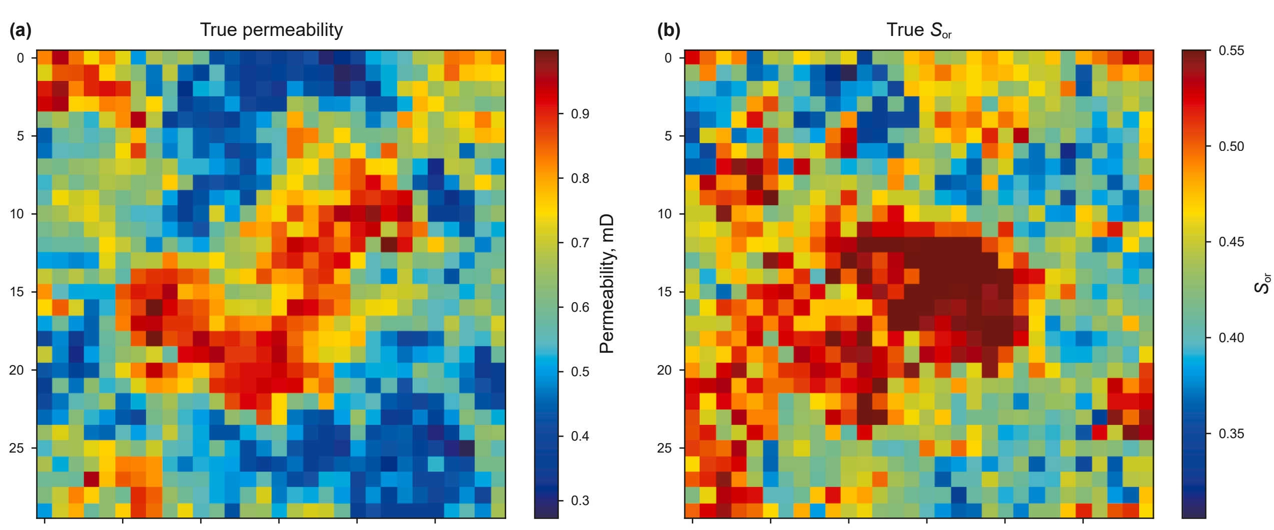

Fig. 3. **(a)** Permeability k and **(b)** S_{or} distributions. The injector and producer are placed at the lower left and upper right corner.

calibration by the workflow. The initial oil saturation $S_{o,i}$ is set to be constant 0.7 to allow oil production at the early stage.

During the PITT simulation, two tracers with distinct partitioning coefficients were co-injected for 2 days at a unified concentration of 1. The partition coefficients for tracers 1 and 2 were 0.4 and 0 respectively.

The simulation result of the case is shown in Fig. 4. The observed data exhibits dynamic behavior in a heterogeneous reservoir. The injection pressure undergoes a rapid initial decline, followed by a brief increase coinciding with water breakthrough. Correspondingly, the water production rate follows a multi-stage trend: a sharp initial rise, a temporary decrease as high-permeability layers water out, and a subsequent increase as the flood front advances through secondary layers before stabilizing. This complex profile indicates an effective sweep of mobile oil, driving the reservoir to residual oil saturation in a manner consistent with field observations. This interpretation is further corroborated by the produced tracer data, which displays clear chromatographic separation of the peaks as a direct result of their differing partitioning coefficients.

3.2. Initialization

An initial ensemble comprising 100 reservoir models was generated using the same method to represent the prior uncertainty in the spatial distributions of k and S_{or}. Each ensemble member was constructed using Gaussian Random Fields. The statistical parameters of the Gaussian Random Fields, including the mean value, correlation angle, and correlation lengths in the x and y directions (L_x,L_y), were varied randomly across the ensemble to produce diverse geological realizations.

Numerical simulations were performed for each ensemble member using the UTCHEM simulator. The resulting prior simulation results are shown in Fig. 4. Q_w is the water production rate as a function of time, the other two plots are the unified concentrations for tracer 1 and tracer 2 in the production wells. The tracer curves exhibited significant deviations from the observed data. This discrepancy is primarily attributed to the presence of a high-conductivity channel in the actual reservoir system, which facilitates preferential flow paths. Consequently, tracer breakthrough in the true system occurred earlier compared to the prior ensemble simulations, as the scale and k of this channel were not adequately represented in the initial realizations. This deliberate initialization from a configuration that poorly matched the observed data served as a stringent test of the data assimilation workflow's capability to improve model predictions and reduce uncertainty.

3.3. Assimilation result

The history matching was performed using the ESMDA with a default setup. Three assimilation steps were used, with a constant covariance inflation factor of 3.0 applied at each step. No

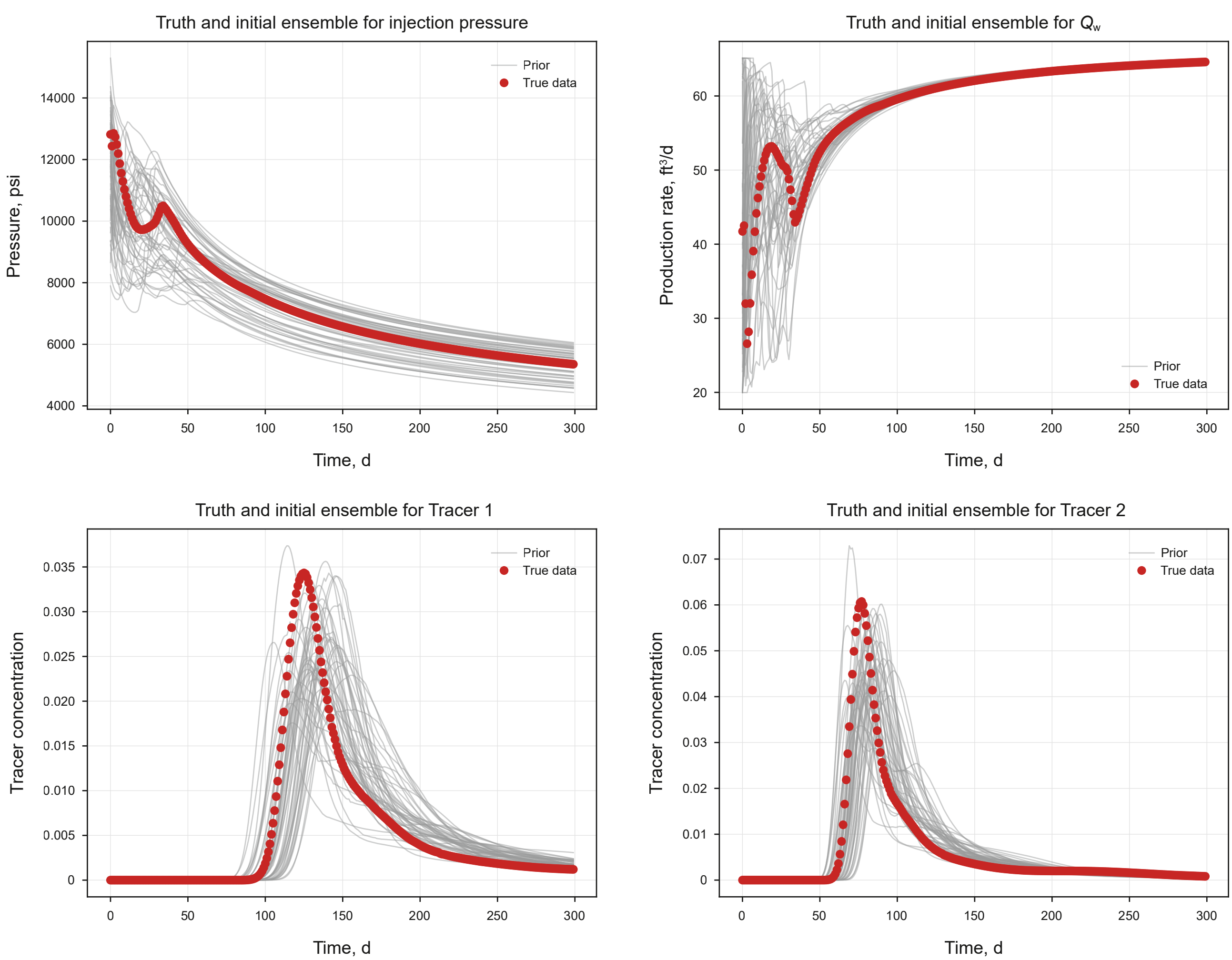

Fig. 4. Comparison of the true data against the prior observations (P_{inj} Q_w, $C_{tracer1}$, $C_{tracer2}$). The red dots represent the observations and the grey lines represent the results of all the prior ensembles.

additional convergence criteria were implemented. The entire workflow was executed on a desktop computer equipped with an Intel i9-12900 16-core processor and completed in 307 s with full parallelization.

The results of the assimilation process are presented (in blue curves) in Fig. 5. As demonstrated, following assimilation, the posterior ensemble simulations exhibit a close match with the observed data. This is particularly evident for the tracer concentration breakthrough curves, where the initial ensembles displayed a noticeable lag relative to the observed data. After assimilation, the posterior ensemble members show strong convergence towards the observed tracer concentration profiles.

These assimilation results are achieved by adjusting the spatial distributions of k and S_{or} within the reservoir model ensembles. A comparison between the initial (prior) and posterior ensemble distributions of k and S_{or} are illustrated in Fig. 6. Initially, the ensemble k fields showed significant deviation from the reference case in terms of both overall scale and characteristic features. The mean k across all initial ensembles was notably low and lacked any discernible spatial trends. Following assimilation, the posterior k fields exhibit a greater representation of the high-conductivity channel feature, more closely resembling the true k distribution, as indicated by the mean k of the posterior ensembles. It is important to note that while the posterior ensembles capture key features of the true k distribution, they also preserve some of the distinctive characteristics inherent to their initializations. The variation among the posterior ensemble members provides a valuable perspective on the remaining uncertainty in the k field.

After assimilation, both the k and S_{or} fields demonstrate significant evolution from their initial states. Specifically, the assimilation process successfully steered the k fields towards accurately capturing the high-conductivity channel present in the reference case. Concurrently, the S_{or} saturation fields began to exhibit the expected clustering distribution in areas influenced by flow. RMSE is 0.1363 for permeability field and 0.0541 for S_{or} field.

The evolution of the ensemble's S_{or} distribution is further illustrated in Fig. 7, which shows the distribution of S_{or} values across the field. The initial (prior) distribution (represented by yellow bars) was distinctly different, characterized by concentrations in specific value ranges and some scattering attributed to limitations in the initialization process. However, after the assimilation process, the resulting posterior distribution (represented by blue bars) shows a significant shift. The initial distinct peaks have diminished, and the distribution now demonstrates a gradual alignment with the true field-observed S_{or} distribution in terms of its shape, range, and overall scale.

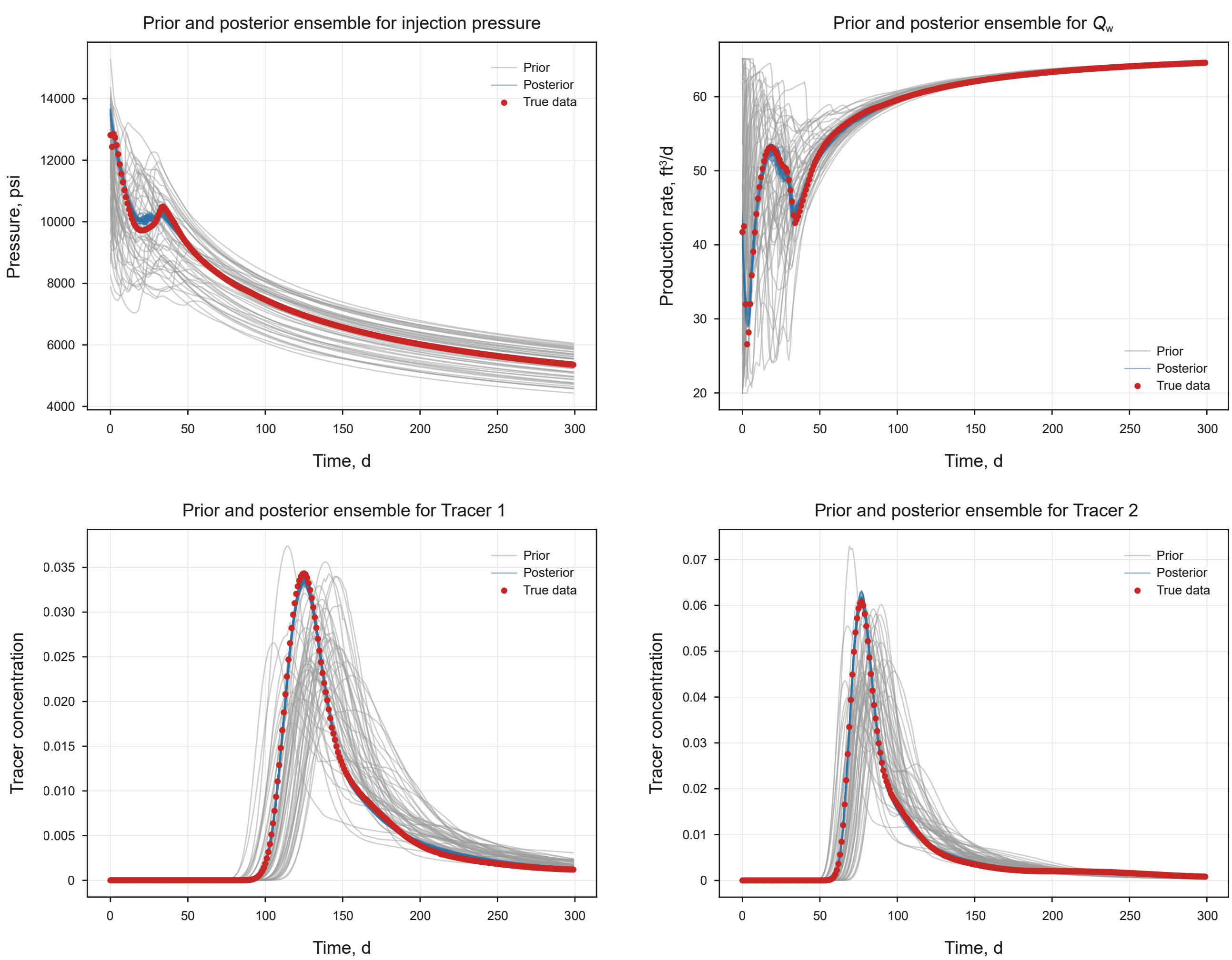

Fig. 5. Assimilation result of the posterior observations (P_{inj} Q_{w}, C_{tracer1}, C_{tracer2}). The red dots represent the observations, the grey lines represent the results of all the prior ensembles, and the blue lines represent the results of all the posterior ensembles after assimilation.

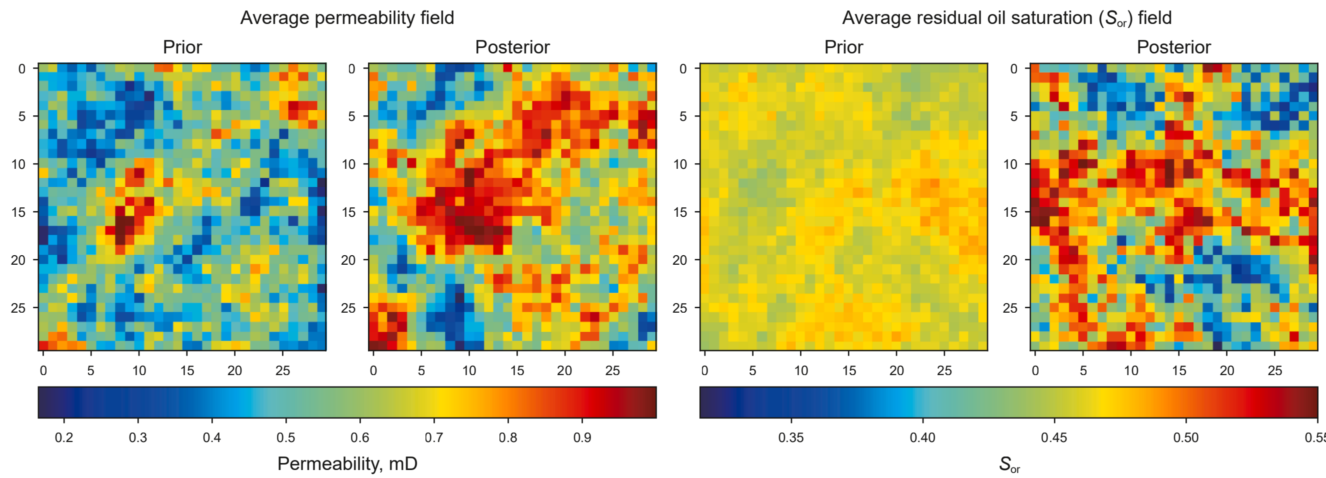

Fig. 6. Evolution of k and S_{or} distributions of the mean of all ensembles and individual prior and after assimilation.

3.4. Uncertainty quantification

In a heterogeneous reservoir, a simple arithmetic average of S_{or} can be misleading. Fluid doesn't flow uniformly through the reservoir; it preferentially moves through high-permeability layers. Therefore, the S_{or} in these high-flow areas has a much greater impact on the overall fluid production and recovery than the S_{or} in tight, low-permeability zones.

To evaluate the average S_{or} relevant to tracer test interpretation or the potential for EOR, it is appropriate to assign a greater significance to S_{or} values within regions actively swept by fluid flow. A permeability-weighted average S_{or} is computed to reflect this idea. The weighted average S_{or} is calculated using the following formula:

$$S_{\mathrm{or,weight}} = \frac{\sum K_i \cdot S_{\mathrm{or},\infty_i^{\circ}}}{K_{\mathrm{ave}}} \tag{8}$$

where k_i and $S_{\mathrm{or},i}$ represent the k and S_{or} of the i-th grid cell, respectively, and k_{ave} is the average permeability of all grid cells. This function calculates a permeability-weighted average to more accurately reflect reservoir flow dynamics. Since injected fluids and tracers preferentially travel through high-permeability zones, the S_{or} in these pathways has a dominant influence on recovery processes. This method yields a more meaningful metric than a simple arithmetic average, which would over-represent regions that are poorly swept by the flood.

The distribution of the permeability-weighted S_{or} values derived from the ensemble members is shown in Fig. 8. Initially, the prior distribution of this weighted S_{or} was relatively broad, spanning approximately 0.40 to 0.49, with a peak concentration around 0.45. Following the data assimilation process, the posterior distribution exhibited significant narrowing, converging to a range of 0.45 to 0.47. Notably, the peak of this post-assimilation distribution demonstrates a close agreement with the independently determined field-scale S_{or} value of 0.46. Rather than presenting a single, potentially unrepresentative value, the ensemble distribution provides a robust quantification of the uncertainty associated with the estimated weighted S_{or}. This probabilistic approach facilitates a more comprehensive and reliable assessment of the predictions. This strong agreement between the assimilated result and the field value highlights the effectiveness of the proposed workflow in accurately characterizing the residual oil saturation distribution.

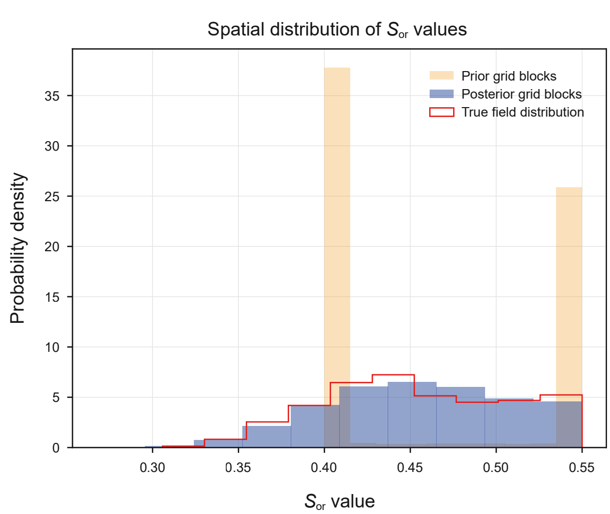

Fig. 7. Field S_{or} distribution of different ensembles. The green, yellow and purple bars represent the distribution of the true value, the prior ensemble and the posterior ensemble.

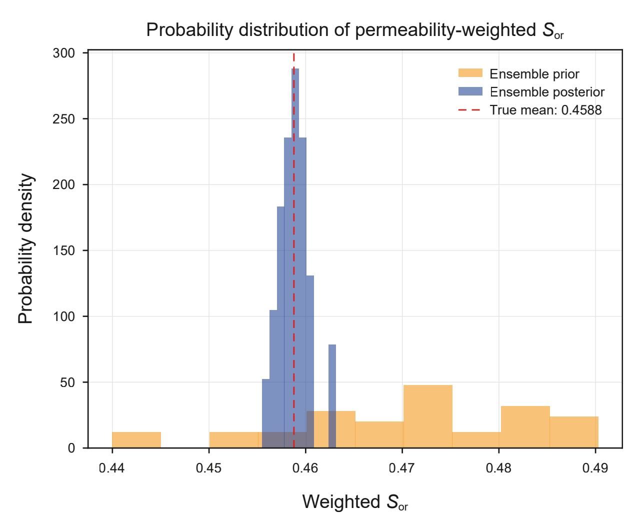

Fig. 8. Probability distribution of S_{or} for all ensembles. The red line is the weighted S_{or} of true field. The yellow and purple bars represent the distribution of weighted S_{or} of all prior and posterior ensembles.

4. Discussion

4.1. Comparison with traditional interpretation result

The traditional approach to interpreting PITT to estimate S_{or} relies on the fundamental principle of chromatographic separation of tracers with different partitioning behaviors between the water and immobile oil phases in a reservoir. These traditional interpretation methods and formulas are based on several simplifying assumptions: 1-D flow, homogeneous formation, equilibrium partitioning and immobile residual oil saturation. Two primary methods have been traditionally used to quantify this retardation and relate it to S_{or}:

Breakthrough curve analysis (time lag analysis): This is the most direct method and involves analyzing the concentration of each tracer in the produced fluids as a function of time, generating breakthrough curves. The relationship between the time lag and S_{or} can be expressed as (Aparecida de Melo et al., 2001):

$$S_{or} = \frac{\left(\frac{\Delta t}{t_c}\right)}{K - 1 + \left(\frac{\Delta t}{t_c}\right)} \tag{9}$$

where $\Delta t = t_p - t_c, t_p$ is the arrival time of the partitioning tracer and t_c is the arrival time of the conservative tracer. K is the oil-water partition coefficient of the partitioning tracer.

Method of moments: This method provides a more rigorous way to analyze the entire breakthrough curve and accounts for the dispersion of the tracer plumes. The first temporal moment of a tracer breakthrough curve is related to the average residence time of the tracer in the reservoir. The first temporal moment (M_1) for each tracer is calculated from its breakthrough curve using the following integral (Jin et al., 1995):

$$M_1 = \frac{\int_0^\infty tC(t)\mathrm{d}t}{\int_0^\infty C(t)\mathrm{d}t} \tag{10}$$

where $C(t)$ is the tracer concentration at time t. The S_{or} is solved by substituting $\left(\frac{\Delta t}{t_c}\right)$ by M_1 in Eq. (9). The method of moments is preferred as it considers the entire concentration history and is less susceptible to distortions in the peak shape caused by dispersion and heterogeneity.

In a perfectly homogeneous system, the time lag observed between a conservative tracer and a partitioning tracer directly corresponds to a single S_{or} value within the swept volume. Conversely, in a heterogeneous system, the composite breakthrough curve at a production well reflects contributions from numerous flow paths, each potentially exhibiting a different lag depending on local S_{or} and flow velocity. Consequently, simple time differences derived from these composite curves represent an average that may not accurately characterize the true spatial distribution of S_{or}, nor does it necessarily equate to a simple arithmetic average. A comparative analysis of results obtained using traditional methods applied to the sample case is presented in Table 1. As demonstrated, reservoir heterogeneity and the presence of mobile oil can lead to significant deviations from the actual field scenario. The analytical solution produced results with a substantial error of 22%–27%. In contrast, our new workflow demonstrates superior accuracy, with an error rate of only 3%. This constitutes a significant error reduction of more than 86%, validating the effectiveness of the new approach. Furthermore, it was

Table 1
Interpretation result comparison with analytic solutions.

Method	S_{or}	Weighted S_{or}
Peak location	0.20	-
Method of momentum	0.25	-
ESMDA workflow (Peak)	0.44	0.46
True value	0.47	0.46

incapable of providing a permeability-weighted S_{or}, which is more representative of the S_{or} within the actively flowing regime. In contrast, the proposed new interpretation workflow provides accurate calibration for both the absolute S_{or} and the permeability-weighted S_{or}.

The new workflow addresses key limitations inherent in traditional PITT interpretation, particularly the unrealistic assumption that the formation is at complete residual oil saturation prior to the test. Achieving such a state solely for the purpose of a tracer test is often impractical or cost-prohibitive in field operations. By relaxing the idealized assumptions of reservoir homogeneity and a unified residual oil saturation, the implementation of the new workflow significantly expands the applicability of PITT to a broader range of reservoir conditions. Moreover, the tracer response data itself serves as a valuable calibration source for characterizing formation heterogeneity.

4.2. Comparison with the use of only production data

There is increasing adoption of the ESMDA algorithm in automated reservoir history matching workflows. Common data types typically include production rates, well pressures, and water-oil ratios. To investigate the impact of data source, a comparative case study was conducted where the same ESMDA workflow was applied, but assimilating only water production rate and injector pressure data. The resulting history match for the P_{inj}, Q_w from this production-only case is presented in Fig. 9. While the workflow achieved a satisfactory match for the observed history, the estimated reservoir properties were not accurate.

The estimation results for permeability and S_{or} derived from this production-only assimilation are shown in Fig. 10. RMSE for Permeability field is 0.2508 and 0.0805 for S_{or} field. The results indicate a significant degradation in model accuracy for Case 2. Specifically, the permeability field estimation suffered an 84% increase in RMSE, while the S_{or} field saw a 49% increase in RMSE, highlighting the superior performance of the methodology used in Case 1. As evident from the figure, the resulting posterior distributions for permeability and S_{or} do not align well with the known or independently validated geological representation of the field. Specifically, the estimated permeability field fails to capture the presence of the high-conductivity channel, and the S_{or} distribution does not exhibit the expected clustering pattern typically observed around such high-permeability, swept areas.

This discrepancy is attributed to the inherent non-uniqueness associated with history matching complex flow behavior in heterogeneous reservoirs. Reliance on a single data source, particularly indirect signals like pressure or bulk production rates, provides insufficient diagnostic power to uniquely constrain the underlying spatial distributions of reservoir properties. Such indirect constraints can lead to significant deviations from the true reservoir state. Furthermore, powerful assimilation algorithms like ESMDA, when constrained by limited or indirect data, may converge to solutions that match the observed data, but produce spurious or geologically unrealistic parameter estimates. The addition of tracer data,

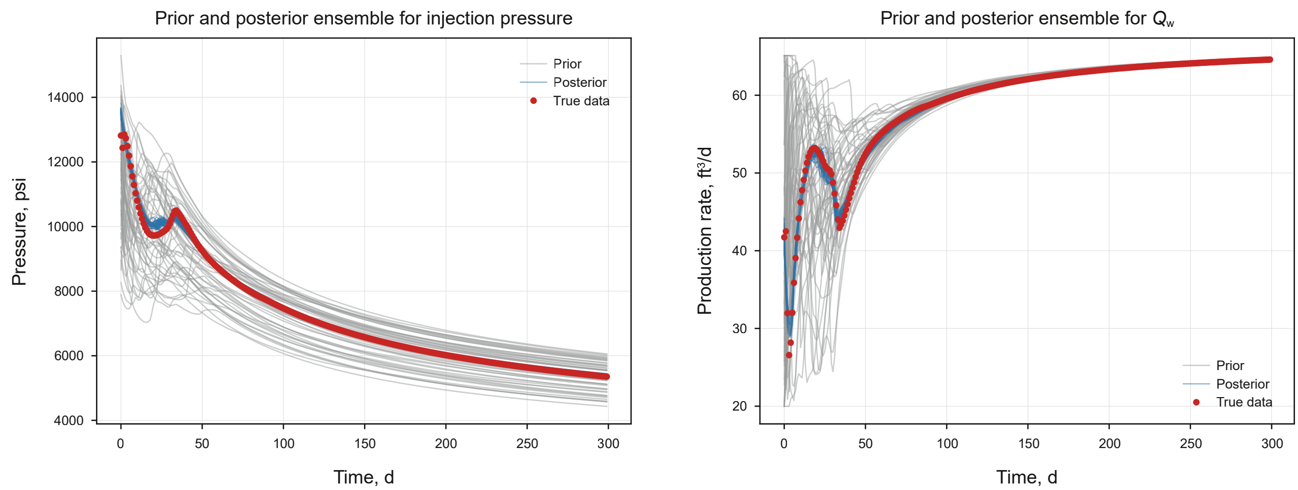

Fig. 9. Assimilation results by injector and water production data only. The red dots represent the observations, the grey lines represent the results of all the prior ensembles, and the blue lines represent the results of all the posterior ensembles after assimilation.

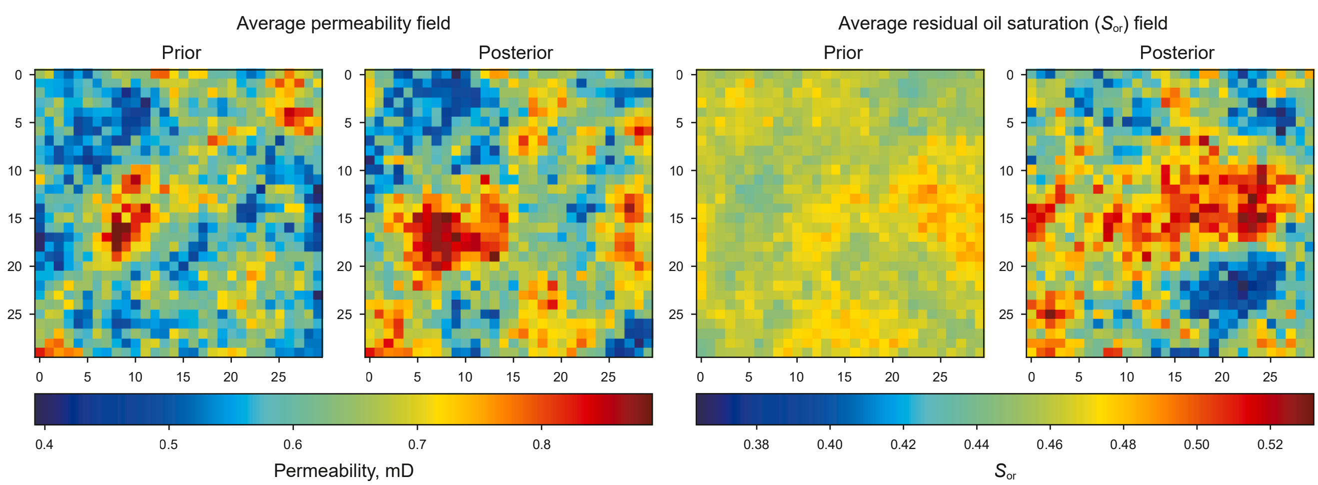

Fig. 10. k and S_{or} assimilation result with only production data.

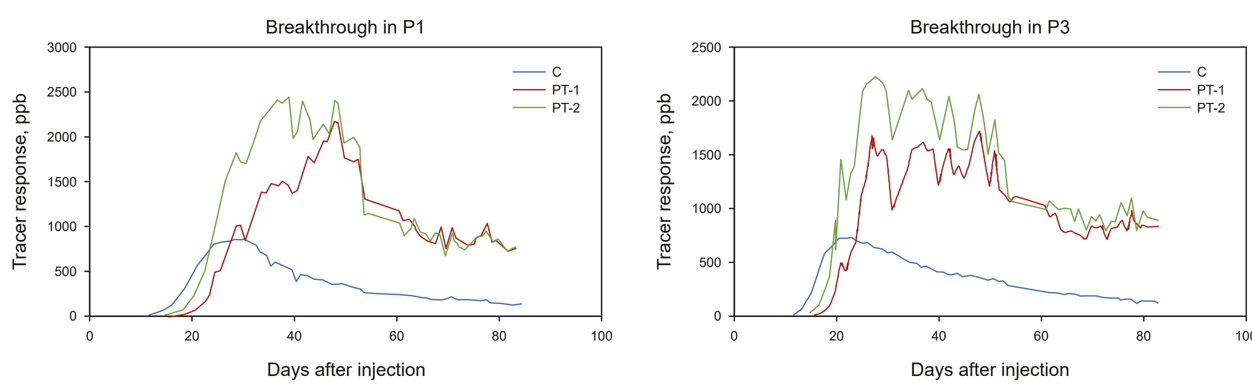

Fig. 11. Example tracer response curves (Guntupalli et al., 2018).

especially from partitioning tracers, offers a more direct measurement of fluid flow pathways and the spatial distribution of S_{or}. The proposed new interpretation workflow leverages the multi-source assimilation capability of ESMDA, integrating both water production rate and tracer data to simultaneously adjust the k and S_{or} distributions. The joint assimilation of these diverse observation types imposes synergistic constraints, enhancing the reliability and resolution of the resulting reservoir characterization.

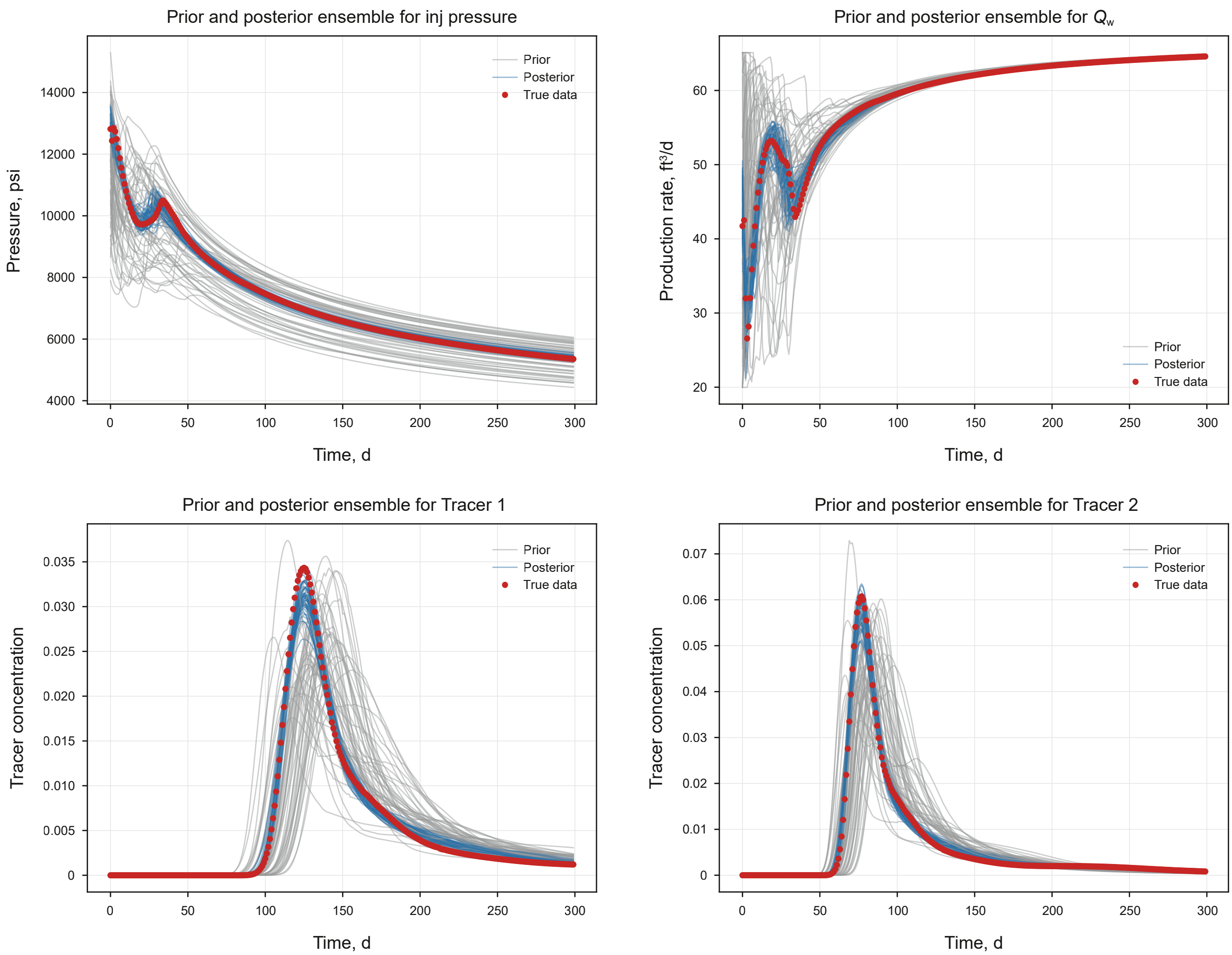

Fig. 12. Assimilation results of observation data with 10 × covariance matrix. The red dots represent the observations, the grey lines represent the results of all the prior ensembles, and the blue lines represent the results of all the posterior ensembles after assimilation.

4.3. Data sampling and noise handling

The observed characteristics of oil field tracer behavior are a direct consequence of the complex and dynamic environment within the reservoir, subject to inherent limitations in the measurement process. Operational factors during tracer tests, including variations in tracer injection rates or concentrations, unscheduled well interventions (such as shut-ins or startups), and alterations in production manifold configurations, can significantly influence subsurface flow patterns and the resulting tracer recovery profiles. Furthermore, the chemical analysis of tracer concentration, often performed at very low detection limits is

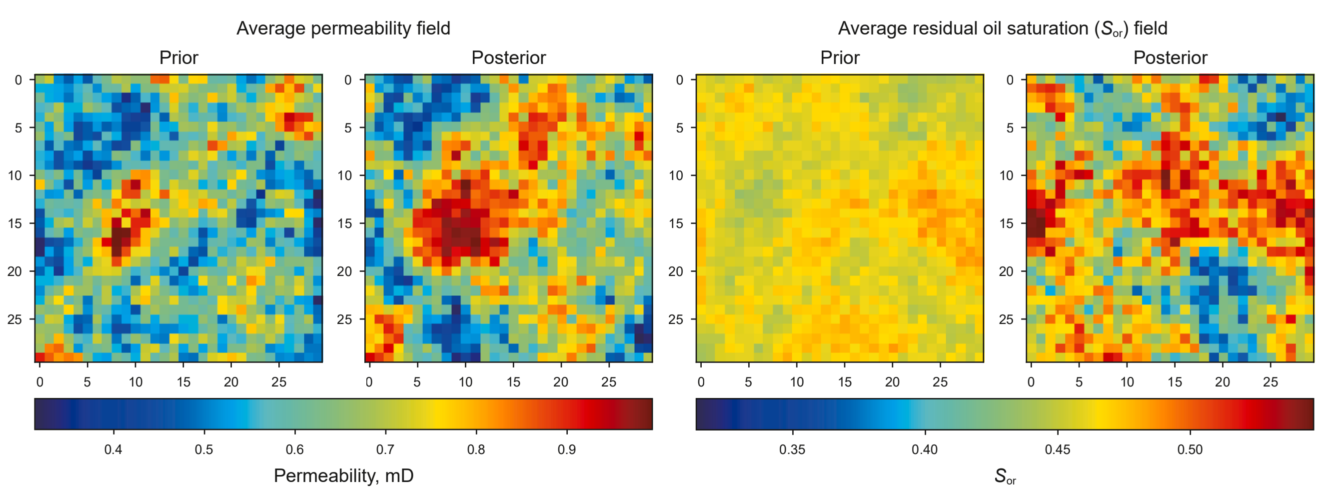

Fig. 13. Assimilation result of k and S_{or} distribution with 10 × covariance matrix.

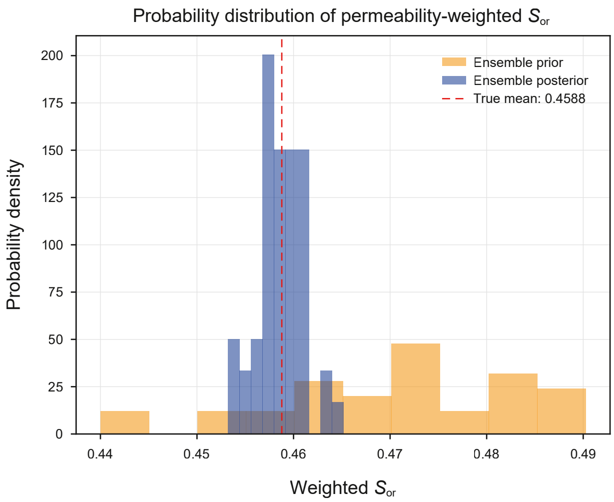

Fig. 14. Probability distribution of S_{or} for all ensembles with 10 × covariance matrix. The red line is the weighted S_{or} of true field. The yellow and purple bars represent the distribution of weighted S_{or} of all prior and posterior ensembles.

susceptible to analytical errors and background interference. These effects can manifest as spurious transient anomalies or deviations in measured tracer concentrations. In contrast to the smooth tracer curves predicted by idealized simulation models, field test results frequently exhibit significant irregularity, as illustrated in Fig. 11. Accurately identifying the peak arrival time for each tracer is challenging in many field scenarios, and quantitatively evaluating the impact of measurement uncertainty on interpretation is also difficult.

The observation error covariance matrix (***R***) plays a critical role in the ESMDA algorithm. This matrix characterizes the statistical properties of the uncertainties associated with the observations. Specifically, it quantifies the uncertainty level of individual observations and describes the correlation structure among the errors of different observations. The structure and magnitude of ***R*** significantly influence the degree to which the assimilated model output conforms to the actual observations; a smaller ***R*** promotes closer adherence to the observational data, whereas a larger ***R*** permits greater deviations between the model predictions and the observations. A comparison demonstrating the effect of varying ***R*** on the interpretation results is presented in Fig. 12. For instance, when the covariance matrix was scaled by a factor of 10 compared to the initial configuration, the resulting posterior ensemble exhibited increased dispersion relative to the original setup. This wider scatter indicates greater variability within the ensembles, reflecting reduced confidence in the observational data.

The assimilation results for k and S_{or} are shown in Fig. 13. The RMSE for Permeability field against true field is 0.1688 and for S_{or} field is 0.0568. Case 3 provides a comparable level of accuracy for matching the S_{or} field, with its RMSE being only 5% higher compare

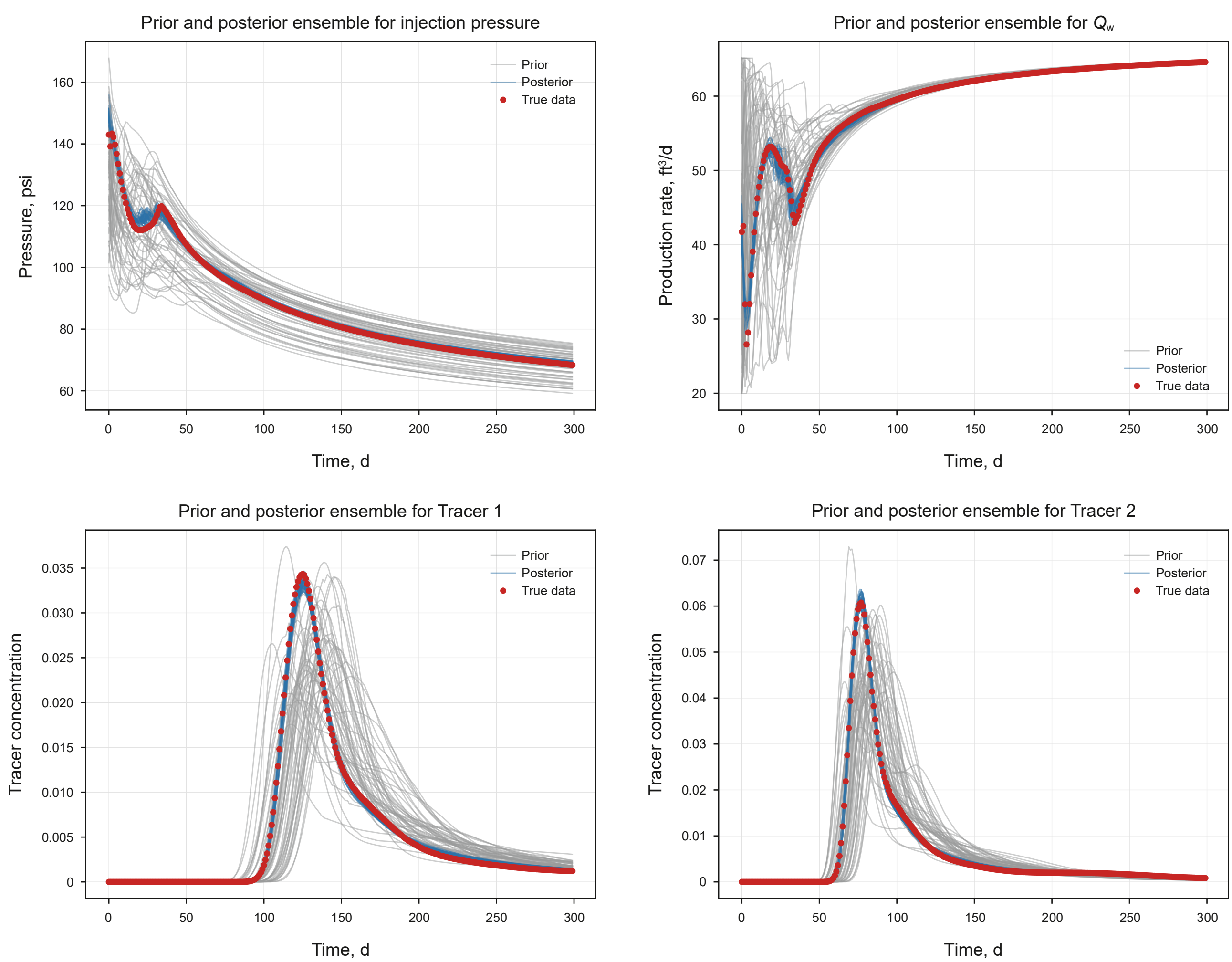

Fig. 15. Assimilation results of observation data. The red dots represent the observations, the grey lines represent the results of all the prior ensembles, and the blue lines represent the results of all the posterior ensembles after assimilation.

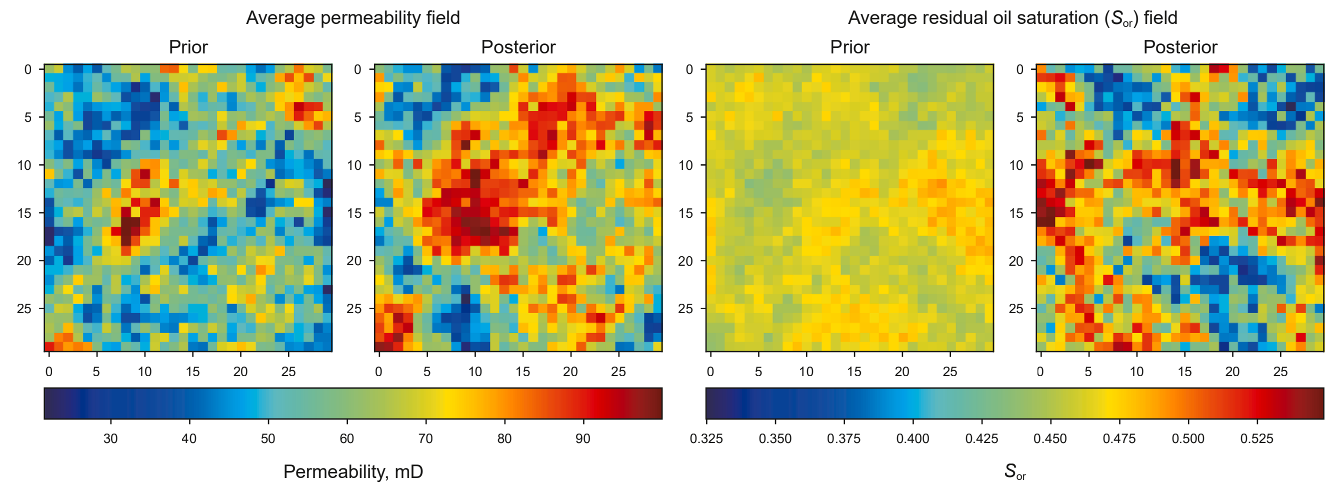

Fig. 16. Assimilation result of k and S_{or} distribution.

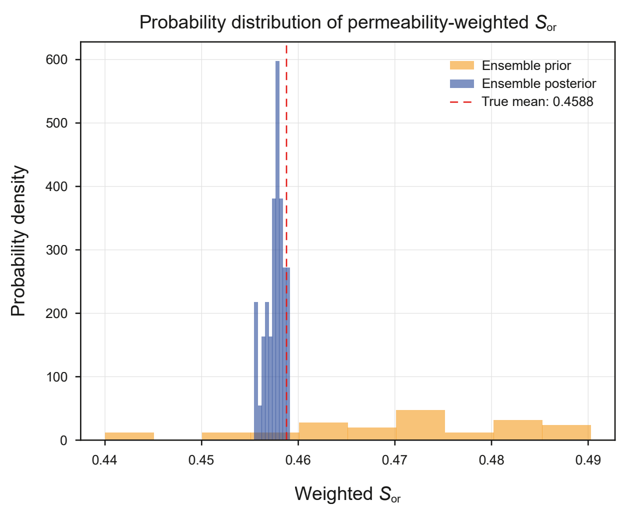

Fig. 17. Probability distribution of S_{or} for all ensembles. The red line is the weighted S_{or} of true field. The yellow and purple bars represent the distribution of weighted S_{or} of all prior and posterior ensembles.

to Case 1. However, Case 3 shows a more significant deviation in matching the permeability field, where the error is 24% greater than in Case 1. The k and S_{or} fields retained key features, such as the inferred high-conductivity channel between the injector and producer wells and the clustered S_{or} distribution. However, these features displayed greater spatial variability.

The weighted S_{or} distribution, shown in Fig. 14, indicates a wider posterior distribution band, spanning approximately 0.44 to 0.50, with a peak value between 0.455 and 0.465. This demonstrates that the proposed workflow enables explicit control over the magnitude of parameter uncertainty by adjusting the observation error covariance matrix. The application of ESMDA, specifically through modification of the observation error covariance matrix, facilitates the management of uncertainty scales and effectively accounts for the impact of data sampling errors and noise, thereby enhancing the robustness of the interpretation.

4.4. Assimilation for a reservoir with a high permeability heterogeneity

To assess the effectiveness of the workflow at high permeability heterogeneity, the permeability range was varied from 1 mD to 100 mD using the same random setup, while the S_{or} distribution remained consistent with the base case. Due to the constant injection rate and production pressure boundary conditions, the overall shape of the simulation results did not change significantly. The assimilation workflow was repeated for 100 ensembles. Fig. 15 shows the P_{inj}, Q_w and the two tracer concentrations. The assimilated permeability and S_{or} distributions can match the true P_{inj}, Q_w and tracer concentrations, demonstrating the algorithm's success.

The permeability and S_{or} spatial distribution before and after assimilation are shown in Fig. 16. The RMSE for permeability field is 33.9 and for S_{or} field is 0.055, which is identical for S_{or} estimation compared to base case. The S_{or} distribution before and after assimilation are shown in Fig. 17. Initial guess was broad, but the assimilation brings it close to the true mean. This sensitivity analysis confirms the workflow's robustness and its applicability across different scales of permeability variation and diverse heterogeneity setups.

5. Conclusions

While the fundamental concept of partitioning inter-well tracer test is simple, its accuracy has long been hampered by the overly simplified assumptions such as homogeneous reservoir. To overcome these limitations, this research introduces a numerical interpretation workflow integrating UTCHEM with the ESMDA algorithm. This advanced framework calibrates the spatial distributions of permeability and S_{or} by jointly assimilating fluid production rate, pressure and tracer concentration data. We demonstrate the workflow's superior performance by comparing it against traditional interpretation methods and a history-matching case without tracer data. Furthermore, a sensitivity analysis on key geological and algorithmic parameters validates its robustness for real-world applications. This work expands the role of PITT from a single saturation measurement into a comprehensive tool for evaluating formation heterogeneity (permeability and oil saturation distributions). The integrated approach offers a cost-effective method for improving inter-well characterization for S_{or} (or NAPL saturation) estimation. The following conclusions are drawn from this study.

1. The proposed workflow successfully integrates multi-source data using ESMDA to generate high-resolution estimates of k and S_{or} fields.

2. PITT is a powerful tool for the simultaneous characterization of both inter-well permeability and S_{or}.
3. A permeability-weighted S_{or} is shown to be a more robust metric for assessing a reservoir's production potential than a simple volumetric average.
4. The inclusion of partitioning tracer data significantly improves the accuracy and resolution of reservoir models developed within a data assimilation framework.
5. By co-assimilating production data, the workflow mitigates the underestimation of S_{or} by analytical solution, a known limitation of traditional analytical PITT interpretation methods.
6. The ensemble-based ESMDA framework provides probabilistic forecasts, enabling rigorous uncertainty quantification of the estimated reservoir properties even with sparse and noisy data.

CRediT authorship contribution statement

Zi-Hao Zhao: Writing – original draft, Validation, Software, Methodology, Investigation, Formal analysis, Data curation, Conceptualization. **Yu-Hao Ou:** Visualization, Methodology, Formal analysis. **Cun-Qi Jia:** Visualization, Validation, Methodology, Formal analysis. **Ruo-Yu Li:** Visualization, Software, Methodology, Formal analysis. **Kishore Mohanty:** Writing – review & editing, Supervision, Project administration, Methodology, Funding acquisition.

Code availability section

The software UTCHEM is available at: https://csee.engr.utexas.edu/research/industrial-affiliate-programs/chemical-enhanced-oil-recovery/ut-chem-simulator.

Declaration of competing interest

The authors declare that they have no known competing financial interests or personal relationships that could have appeared to influence the work reported in this paper.

Acknowledgements

This project was partly funded by the Chemical EOR IAP at The University of Texas at Austin.

References

Agca, C., Pope, G.A., Sepehrnoori, K., 1990. Modelling and analysis of tracer flow in oil reservoirs. J. Petrol. Sci. Eng. 4 (1), 3–19. https://doi.org/10.1016/0920-4105(90)90042-2.

Allison, S.B., Pope, G.A., Sepehrnoori, K., 1991. Analysis of field tracers for reservoir description. J. Petrol. Sci. Eng. 5 (2), 173–186. https://doi.org/10.1016/0920-4105(91)90066-V.

Aparecida de Melo, M., de Holleben, C.R., Almeida, A.R., 2001. Using tracers to characterize petroleum reservoirs: Application to carmopolis field, Brazil. In: Presented at the SPE Latin American and Caribbean Petroleum Engineering Conference, SPE-69474-MS. https://doi.org/10.2118/69474-MS.

Brigham, W.E., Smith Jr., D.H., 1965. Prediction of tracer behavior in five-spot flow. In: Presented at the Conference on Production Research and Engineering. https://doi.org/10.2118/1130-MS. SPE-1130-MS.

Cubillos, H., Yuste, E., Bozorgzadeh, M., Montes, J., Mayorga, H., Bonilla, S., et al., 2015. The value of inter-well and single well tracer technology for de-risking and optimizing a ceor process – Caracara field case. In: Presented at the EUROPEC 2015. https://doi.org/10.2118/174397-MS.

Dwarakanath, V., Deeds, N., Pope, G.A., 1999. Analysis of partitioning interwell tracer tests. Environ. Sci. Technol. 33 (21), 3829–3836. https://doi.org/10.1021/es990082v.

Evensen, G., Raanes, P.N., Stordal, A.S., Hove, J., 2019. Efficient implementation of an iterative ensemble smoother for data assimilation and reservoir history matching. Front. Appl. Math. Stat. 5, 47. https://www.frontiersin.org/journals/applied-mathematics-and-statistics/articles/10.3389/fams.2019.00047.

Gu, Y., Oliver, D.S., 2005. History matching of the PUNQ-S3 reservoir model using the ensemble kalman filter. SPE J. 10 (2), 217–224. https://doi.org/10.2118/89942-pa.

Guntupalli, S., Chatterjee, M., Svec, Y., Al-Shuaili, K., Amri, M., Pugla, S., Hewitt, P., 2018. Application of interwell partitioning tracers for evaluating the effectiveness of chemical EOR in field A in Southern Sultanate of Oman: A case study. In: the Abu Dhabi International Petroleum Exhibition & Conference 2018, SPE-192649-MS. https://doi.org/10.2118/192649-MS.

Guo, Q., Shi, X., Kang, X., Hao, S., Liu, L., Wu, J., 2021. Evaluation of the benefits of improved permeability estimation on high-resolution characterization of DNAPL distribution in aquifers with low-permeability lenses. J. Hydrol. 603, 126955. https://doi.org/10.1016/j.jhydrol.2021.126955.

Hartog, N., Cho, J., Parker, B.L., Annable, M.D., 2010. Characterization of a heterogeneous DNAPL source zone in the Borden aquifer using partitioning and interfacial tracers: Residual morphologies and background sorption. J. Contam. Hydrol. 115 (1), 79–89. https://doi.org/10.1016/j.jconhyd.2010.04.004.

Hirtz, P.N., Kunzman, R.J., Broaddus, M.L., Barbitta, J.A., 2001. Developments in tracer flow testing for geothermal production engineering. Geothermics 30 (6), 727–745. https://doi.org/10.1016/S0375-6505(01)00023-2.

Huseby, O., Hartvig, S.K., Jevanord, K., Dugstad, Ø., 2015. Assessing EOR potential from partitioning tracer data. In: SPE Middle East Oil and Gas Show and Conference, SPE-172808-MS.

Illiassov, P.A., Datta-Gupta, A., 2002. Field-scale characterization of permeability and saturation distribution using partitioning tracer tests: The ranger field, Texas. SPE J. 7 (4), 409–422. https://doi.org/10.2118/81198-pa.

Jin, M., Delshad, M., Dwarakanath, V., McKinney, D.C., Pope, G.A., Sepehrnoori, K., et al., 1995. Partitioning tracer test for detection, estimation, and remediation performance assessment of subsurface nonaqueous phase liquids. Water Resour. Res. 31 (5), 1201–1211. https://doi.org/10.1029/95WR00174.

Keller, Y.A., Келлер, Ю.А., Александрович, К.Ю., Uskov, A.A., Усков, А.А., Александрович, У.А., 2023. The methods for evaluating the efficiency of EOR by SWCTT & PITT tracer tests. Kazakhstan J. Oil Gas Ind. 5 (1), 47–56. https://doi.org/10.54859/kjogi108627.

Liu, P., Zhang, K., Yao, J., 2023. Reservoir automatic history matching: Methods, challenges, and future directions. Adv. Geo-Energy Res. 7 (2), 136–140. https://doi.org/10.46690/ager.2023.02.07.

Oliver, D.S., Chen, Y., 2011. Recent progress on reservoir history matching: A review. Comput. Geosci. 15 (1), 185–221. https://doi.org/10.1007/s10596-010-9194-2.

Pu, C., Jing, C., He, Y., Gu, X., Zhang, Z., Wei, J., 2016. Multistage interwell chemical tracing for step-by-step profile control of water channeling and flooding of fractured ultra-low permeability reservoirs. Petrol. Explor. Dev. 43 (4), 679–688. https://doi.org/10.1016/S1876-3804(16)30079-9.

Saad, N., Pope, G.A., Sepehrnoori, K., 1989. Simulation of big muddy surfactant pilot. SPE Reserv. Eng. 4 (1), 24–34. https://doi.org/10.2118/17549-PA.

Sanni, M., Al-Abbad, M., Kokal, S., Dugstad, Ø., Hartvig, S., Huseby, O., 2018. Pushing the envelope of residual oil measurement: A field case study of a new class of inter-well chemical tracers. J. Petrol. Sci. Eng. 163, 538–545. https://doi.org/10.1016/j.petrol.2017.12.076.

Sanni, M.L., Al-Abbad, M.A., Kokal, S.L., Hartvig, S., Olaf, H., Jevanord, K., 2015. A field case study of Inter-well chemical tracer test. In: SPE International Symposium on Oilfield Chemistry. https://doi.org/10.2118/173760-MS.

Suva, J.A.K., Mariner, P.E., Meinardus, H.W., Ginn, J.S., 2003. Monitoring partitioning tracer testing and surfactant flooding by in-line gas chromatography techniques. Groundw. Monit. Remed. 23 (1), 85–92. https://doi.org/10.1111/j.1745-6592.2003.tb00786.x.

Tang, Joseph S., 1995. Partitioning tracers and In-situ fluid-saturation measurements. SPE Form. Eval. 10 (1), 33–39. https://doi.org/10.2118/22344-PA.

Tang, Joseph S., 2005. Extended Brigham model for residual oil saturation measurement by partitioning tracer tests. SPE J. 10 (2), 175–183. https://doi.org/10.2118/84874-PA.

Tang, J.S., Harker, B., 1991. Interwell tracer test to determine residual oil saturation in a gas-saturated reservoir. Part I: Theory and design. J. Can. Petrol. Technol. 30 (3). https://doi.org/10.2118/91-03-08.

Tayyib, D., Al-Qasim, A., Kokal, S., Huseby, O., 2019. Overview of tracer applications in oil and gas industry. In: SPE Kuwait Oil & Gas Show and Conference. https://doi.org/10.2118/198157-MS.

Velasco-Lozano, M., Balhoff, M.T., 2023. Modeling of chemical tracers for two-phase flow in capillary-dominated porous media. Fuel 339, 127421. https://doi.org/10.1016/j.fuel.2023.127421.

Zhang, K., Yu, H.-Q., Ma, X.-P., Zhang, J.-D., Wang, J., Yao, C.-J., et al., 2022. Multi-source information fused generative adversarial network model and data assimilation based history matching for reservoir with complex geologies. Pet. Sci. 19 (2), 707–719. https://doi.org/10.1016/j.petsci.2021.10.007.

Zhang, W., Sun, X., Wang, L., Li, Y., Zhao, G., Meng, W., 2023. Conductivity evaluation of horizontal wells in coalbed methane reservoirs: Applicability of micromaterial tracer testing technology. ACS Omega 8 (1), 1131–1139. https://doi.org/10.1021/acsomega.2c06542.

Zhao, Z., Yang, H., Wu, J., Chang, C., Sun, H., Sepehrnoori, K., et al., 2021. Fracture diagnosis with distributed temperature sensing using thermal embedded discrete fracture model (EDFM). Present. 55th U.S. Rock Mech. Geomech. Symp.

Zhao, Z., Ou, Y., Jia, C., Mohanty, K.K., 2025. A novel workflow for interpretation of single-well tracer tests. In: Offshore Technology Conference. https://doi.org/10.4043/35589-MS.